

Submitted to The Astronomy Letters.

Activity of the Soft Gamma Repeater SGR 1900+14 in 1998 from Konus-Wind Observations:

2. The Giant August 27 Outburst.

E.P.Mazets¹, T.L.Cline², R.L.Aptekar¹, P.Butterworth², D.D.Frederiks¹, S.V.Golenetskii¹,
V.N.Il'inskii¹, V.D.Pal'shin¹

ABSTRACT

The results of observations of the giant 1998 August 27 outburst in SGR 1900+14 are presented. A comparison is made of the two extremely intense events on August 27, 1998 and March 5, 1979. The striking similarity between the outbursts strongly implies a common nature. The observation of two giant outbursts within 20 years from different sources suggests that such events occur in an SGR once every 50–100 years.

¹Ioffe Physical-Technical Institute, St.Petersburg, 194021, Russia. Mazets@pop.ioffe.rssi.ru

²Goddard Space Flight Center, Greenbelt, MD 20771, USA.

1. INTRODUCTION

The discovery of soft recurrent bursts started with the observation of the famous gamma-ray outburst on March 5, 1979 (Mazets et al., 1979a). On the next day, the Konus experiment on the Venera 11 and 12 spacecraft detected the first recurrent burst arriving from the same source (Mazets et al., 1979a). The number of detected recurrent bursts increased subsequently to 16 (Golenetskii et al., 1984). At the end of March 1979, the Konus experiment discovered and localized a second recurrent burster, B1900+14 (Mazets et al., 1979b), and it is the new reactivation of the latter that is being considered in the present paper.

Recurrent bursts have been observed from these and more recently discovered soft gamma repeaters during rare periods of activity separated by long quiet intervals. However the March 5 event remained until recently the only one of its kind. Accordingly, the question of the extent to which the 1979 March 5 event is characteristic of the activity of soft gamma repeaters, of whether such events are typical for all SGRs, or this giant outburst was a unique episode in the history of one object only, remained unclear. Arguments for both the first (Mazets et al., 1982) and second (Norris et al., 1991; Fenimore et al., 1996) alternative were put forward.

An unambiguous answer to this question was obtained on August 27, 1998, when several spaceborne experiments detected a giant outburst in SGR 1900+14, which was strikingly similar to the one that had occurred in SGR 0526-66 on 1979, March 5 (Cline et al., 1998; Hurley et al., 1999; Feroci et al., 1999).

In this paper, we are going to consider in detail the results of the Konus-Wind observations of the 1998 August 27 outburst and to compare it with the 1979 March 5 event.

2. OBSERVATIONS

The outburst on August 27, 1998 has no precedents in its intensity. The peak flux of hard photons with energies > 15 keV is considerably in excess of the level observed heretofore from any known cosmic sources. The overall time history of the burst is displayed in Fig. 1. As in the March 5 event, the burst starts with a narrow radiation pulse, which falls off rapidly to become a slowly decaying, coherently pulsating tail.

We will consider in detail this and other characteristic stages in the development of the event.

a) Initial pulse and the $T - T_0 < 1$ s region

The Konus-Wind cosmic gamma-ray burst spectrometer (Aptekar et al., 1995) starts a program of detailed measurements from the instant T_0 at which the trigger signaling the arrival of a burst is generated. This program includes measurement of the burst time history in three energy windows G1 (15–50 keV), G2 (50–250 keV), and G3 (250–1000 keV) with a time resolution of 2 to 256 ms. The burst prehistory, i.e. some measurements preceding T_0 , is also stored. The trigger signal is generated in the second energy window G2 (50–250 keV) after the count rate has risen in a short time by ~ 7 standard deviations. The T_0 signal also initiates measurements of multichannel energy spectra with automatic adaptation of the accumulation time to the current count rate.

Figure 2 presents the initial part of the burst profile recorded within $T - T_0$ from -0.5 to 1 s. A weak precursor is observed in the soft-energy window 0.45 s before T_0 . As seen from the graph, the number of additional counts required to generate the trigger arrives in as short a time as 4 ms, so that the intensity rises very rapidly. In another 4 ms, no counts are detected in any window. This implies that the radiation intensity becomes so high only 4 ms after T_0 that the count-rate channel completely overloads.

The instrument remains silent for a time, to revive again after ~ 200 ms. The dead time and pulse pile-up effects in the detector distort the real picture so strongly as to make correcting the data obtained an extremely difficult problem. To solve it, thorough laboratory studies of counting losses and pulse superposition effects were carried out on the spare hardware of the instrument at incident fluxes of 10^6 – 10^7 photons s^{-1} and higher. The measurements were performed with radioactive sources and X-ray equipment, whose radiation permitted a satisfactory simulation of the required continuous spectra. A numerical model of the instrument response to high radiation fluxes was also made. Because of the importance of the data obtained for a correct evaluation of the event energetics, we will discuss them in detail.

Under normal conditions and with most devices, the total photon flux N incident on a detector is related to the recorded count rate n through the obvious expression $1/n - 1/N = \tau$, where τ is the instrument dead time. For $N \gg 1/\tau$, n should tend to the limiting value $n = 1/\tau$ and become independent of N . Figure 3 exemplifies the results of both laboratory measurements and numerical simulation of the count rates in the G1, G2 and G3 windows, and of their sum, as functions of input intensity for a spectrum representing a broad line with an energy ~ 100 keV. As can be seen from the graphs, the standard $n(N)$ relationship holds until $N \sim 10^6$, but as the intensity N continues to increase, the detected number of counts n drops dramatically to finally vanish altogether. This behavior has a straightforward explanation. For high N , overlap of individual pulses

in the detector gives rise to the formation and growth of a dc electric current component. Single-photon counts start to be replaced by detection of output-signal fluctuations, which causes extremely strong distortions of the measured spectrum. Indeed, the count rate in the third, hard window displayed in Fig. 3 is totally due to scintillation pile-up in the detector. As the input flux continues to increase, the growth of the fluctuating dc signal at the amplifier output becomes limited by the power supply voltage. After this saturation level has been reached, the count rate drops dramatically, to vanish altogether when it is exceeded. Laboratory studies also revealed the important roles played by two aftereffects, which must be taken into account when the intensity undergoes sharp variations near the saturation level. The first of these is associated with the afterglow of the long-lived phosphorescence component in the NaI(Tl) crystal, which results in time profile tailing. The second effect is connected with the slow response of the PMT high-voltage stabilization circuit. As a result, following large intensity jumps near shut-down the photomultiplier gain can deviate from the nominal value for 30–40 ms. It is this instrumental effect reproduced in laboratory conditions that accounts for the short-period appearance of counts during the interval $T - T_0 = 20 - 30$ ms.

Note the good agreement between direct measurements and numerical simulation of the $n(N)$ relations. This is a very important point. The pattern of the $n(N)$ relations for each of the three energy windows G1, G2, and G3 turns out to be strongly sensitive to the shape of the incident energy spectrum. Hence by comparing the observed count rates n_1 , n_2 , and n_3 one can reliably estimate not only the incident intensity but the spectral hardness as well. The possibility of spectral shape selection in laboratory conditions was limited, but the agreement between the results of direct measurements and simulation permits one to apply the simulation of the $n(N)$ relations to spectra of any shape.

Turning back now to the August 27 event and Fig. 1, we may conclude that while the problem of reproducing the shape of the burst profile during the first second after T_0 is very difficult, it can be solved, except for the intervals of total shut-down. We have also been able to obtain important limiting estimates for the $T - T_0 = 0 - 0.2$ s interval. Note the following two important points. First, during the last few ms of the prehistory before T_0 the count rates are still not high enough to become distorted. Their ratio in the three energy windows permits one to estimate the spectral hardness at the very beginning of the burst, which was found to be very high, corresponding for a $\propto E^{-1} \exp(-E/kT)$ spectrum to $kT \sim 200$ keV. Second, close to saturation the detector starts to operate as a calorimeter. The dc component of the PMT output current is proportional to the average photocathode illumination by scintillations, i.e. to the total energy released in the detector per unit time. The output current corresponding to saturation for a given spectrometer gain is known. Numerical simulation permits one to also take into account the fluctuations in the PMT

output current, whose level depends on the hardness of the incident photon spectrum. Hence we can determine with a high accuracy the incident energy flux on the detector corresponding to complete suppression of counting. For instance, for incident photon spectra with $kT = 30$ and 300 keV it was found to be 2.4×10^{-2} and 3.1×10^{-2} erg cm $^{-2}$ s $^{-1}$, respectively. Thus the lower limit of the burst energy flux at total shut-down is established reliably.

Interestingly, total overload of the Konus-Wind detectors has been observed to occur more than once in so-called imitation bursts, which are produced by ultrarelativistic multi-charged cosmic-ray nuclei interacting with the NaI(Tl) crystal. An instantaneous release of a tremendously high energy in the crystal is accompanied by a slowly decaying afterglow of the long-lived phosphorescence component with decay time $\tau \sim 100 - 150$ ms (Koički S., Koički A., Ajdačić, 1973). The PMT output current fluctuations are detected as individual X-ray photons. Figure 4 illustrates a moderately strong imitation burst observed on July 22, 1997. The output current due to the particle energy loss instantly overloads the amplifier. After the current has decayed below the saturation level, an enormous count rate appears in the G1 window. This example (compare with Fig. 2) also reveals a short-lived appearance of counts due to the slow response of the PMT power-supply stabilization system. Figures 2 and 4 differ radically in the count-rate levels in the G2 and G3 hard windows. This results from differences in the amplitude of fluctuations in the output current and their scatter, caused by the fact that the saturation in the August 27 event occurs as a result of superposition of narrow scintillation trains caused by hard gamma photons, whereas the imitation burst is actually a sum of an enormous number of small signals produced by individual phosphorescence photons.

Within the $T - T_0 = 0.2 - 1$ s interval, the photon flux incident on the detector is still very high. It undergoes strong and sharp variations both in intensity and spectral composition. Four detector spectra were obtained within this interval with a 0.256 s accumulation time. Such averaging is too coarse to allow determination of fast changes in the intensity and hardness. Nevertheless, Fig. 5 shows convincingly that on the average the burst radiation hardness within the $T - T_0 = 0.512 - 0.768$ s interval is substantially higher.

Numerical simulation offers the possibility of reconstructing the initial levels of intensity and hardness with a high temporal resolution. We are speaking about reconstruction rather than introduction of corrections, because the measured and real intensities may differ by orders of magnitude. The procedure of reconstruction consists essentially in finding for each three count rates in the three windows n_i (see Fig. 2) the pair of values of N and kT such that the calculated values of $n_i(N, kT)$ provide the best fit to the measurements. One has to understand by the kT parameter here the hardness characteristic of the burst energy

spectrum adopted in the calculations for a given instant of time. The spectral shape used most frequently is that of thermal bremsstrahlung radiation. Power-law and Band (1993) spectra were also tried.

The first second of the burst time history reconstructed using this procedure is displayed in Fig. 6. Also shown is the variation of kT . We readily see that the initial pulse decays nonmonotonically. The smoothness of the exponential falloff ($\tau \sim 35$ ms) is broken by two additional peaks in intensity. The radiation spectrum varies very strongly. In the very beginning of the pulse ($T - T_0 = 0 - 4$ ms), $kT \sim 300$ keV. The radiation in the decaying part turns out to be very soft, $kT \sim 20$ keV. By the time $T - T_0 \sim 350$ ms, the radiation intensity drops down to $\sim 5 \times 10^5$ photons s^{-1} . The kT remains low, ~ 20 keV. After this the intensity begins to grow again to increase by an order of magnitude by the time $T - T_0 = 550$ ms. The temperature increases to 250 keV. Finally, the intensity falls off to become a long, slowly decaying tail. The dashed line at the top of the initial pulse specifies the lower intensity limit corresponding to instrument shut-down. The real intensity in the initial pulse considerably exceeded this limit, possibly by a large factor. The initial pulse apparently ends by the time $T - T_0 \sim 300$ ms. The new, nearly tenfold increase in intensity and, most significantly, the sharp growth in radiation hardness possibly indicate a manifestation of some new aspects of the burst process and, perhaps, of new additional sources of energy.

Thus the first second in the outburst time history appears to have been very complex. It should be noted that information on the initial phase of the August 27 burst observed from Ulysses (Hurley et al., 1999) and BeppoSAX (Feroci et al., 1999) was irretrievably lost.

b) Transition region, $T - T_0 = 1 - 35$ s, and subsequent pulsations

Within this time interval (Fig. 7), the intensity falls off slowly. The monotonic course of the decay is broken by fairly strong variations revealing a periodicity with $P = 5.16$ s. The observed count-rate level allows straightforward dead-time corrections. Figure 7 also shows the variation of the count-rate ratio in two energy windows, which characterizes spectral hardness. The spectra obtained at the beginning and at the end of this interval are illustrated by Fig. 8.

Starting from the 35th second, the strict periodicity of the radiation becomes increasingly distinct (Fig. 7). The pulsation amplitude increases strongly. The pattern of pulsations does not remain stable. In the beginning of this region, the $P = 5.16$ s period

is represented by four separate peaks. The peaks decrease gradually in relative amplitude. By the end of the observations, they become barely visible, but the modulation at the fundamental frequency is still seen. The hardness curve likewise behaves in a very complex manner. Averaged over of the period, the hardness remains practically constant. This is corroborated by the spectral measurements (Fig. 8), which yield values of kT within 23 ± 3 keV, but the pulsations are accompanied by small-scale hardness variations. During the first 100 s of the burst, the hardness clearly correlates with the intensity of individual peaks. Nearer the end of the burst, the situation reverses. The hardness of the radiation component modulated at the main frequency of 0.194 Hz is observed to be highest at the minima of the intensity.

3. DISCUSSION

The two giant outbursts, observed on March 5, 1979 in SGR 0526-66 and on August 27, 1998 in SGR 1900+14, were strikingly similar. Combined analysis of these events is of considerable interest. Therefore for the sake of convenience we present in Fig. 9 the 1979 March 5 burst profile as observed from the Venera 11 and 12 spacecraft, and in Fig. 10, the time history of the 1998 August 27 event. Each event consists of a short, superintense radiation pulse followed by an exponentially decaying tail. The tail exhibits, in its turn, strictly periodic pulsations, which set in and develop rapidly. Immediately after the initial pulse one observes an intensity increase in the form of a single wave, which is not in phase with the train of periodic pulsations. Fairly fast irregular oscillations appear at the crest of the wave. In both cases the initial pulse is ~ 0.25 s long. Most of the intensity increase occurs during a short time of ~ 2 ms. By contrast, in the August 27 event one observes, besides a weak precursor at the very beginning of the pulse, an 80-ms long slow increase in intensity, and it is this increase that transforms to the steep rise. If such details did exist in the March 5 event, they were below the detection threshold. In this event as seen from Fig. 9, the initially steep rise is replaced by a slower increase of the intensity. Accordingly, the maximum in the pulse is reached in 50–100 ms. One may conjecture that the initial pulse in the August 27 event likewise increased with a slowing down of the rise, judging from the short-time observation of counts within the $T - T_0 = 30 - 40$ ms interval (Fig. 2). We recall that such an effect is possible if the intensity slightly exceeds the saturation level.

In both events, the decay of the initial pulse is close to exponential with a time constant ~ 40 ms. An additional hump is observed in the intensity profile of each event after the initial pulse. In contrast to SGR 0526-66, the distinct recurrent pattern of periodic pulsations in SGR 1900+14 does not set in immediately, but after 35–40 s. However during

this interval the power spectrum likewise exhibits a clearly pronounced peak at a frequency of 0.194 Hz.

The pulsating tails in both events decay with exponential constants of 80–100 s. The behavior of the energy spectra also exhibits a pronounced similarity. The spectrum of the initial pulse in the SGR 0526-66 burst contains a hard component with an emission feature around 400 keV (Mazets et al., 1979a). The pulsations have a soft spectrum with $kT = 30 - 35$ keV, similar to those of the later bursts. Because of the giant intensity of the initial pulse, accurate spectral data for the August 27 event could not be obtained. It has, however, been reliably established that the spectrum at the very beginning of the pulse after T_0 is very hard, $kT \sim 300$ keV, to become very soft, with $kT \sim 20$ keV, in its tail, below the saturation limit. A similar fast spectral evolution during the development and decay of the initial pulse could possibly have occurred in the March 5 event too, and it is the fast spectral variability that accounts for the presence of a hard and a soft component in the resultant spectrum.

It is appropriate to note here that the spectrum of the initial pulse in the March 5 event measured on the Venera spacecraft (Mazets et al., 1979a) was questioned by Fenimore et al (1996). Unfortunately, those authors based their consideration on a wrong assumption that the dead time in the multichannel spectral measurements was ~ 1 ms and that, accordingly, the number of counts accumulated during ~ 200 ms was very small, not more than 200 for the whole spectrum. In fact, the 1 ms-time was the dead time under independent accumulation of counts in each of the 16 spectrometer channels separately, a condition providing reliable spectral measurements.

The second strong intensity rise in the August 27 event, which was accompanied by a sharp increase and decay in hardness, arrived as a single wave at the time $T = T_0 + 0.5$ s. Thereafter the spectral variations became, as in the March 5 burst, quite moderate, with the average value $kT \simeq 25$ keV typical also of the recurrent bursts in SGR 1900+14 remaining constant.

On the whole, the information collected on the two superintense outbursts is not at odds with the assumption that the processes accounting for emission of the narrow initial pulse and the long pulsating tail are separated in the source not only in time but in space as well, as is proposed in the model of Thompson and Duncan (1995).

The characteristics of the two bursts are listed in Table 1. Table 2 contains the burst energetics in the sources. The obvious similarity between the bursts suggests an intimate similarity between the processes involved in their generation.

As follows from the above data, an explosive release of energy which is enormous even

for a neutron star did not produce noticeable changes in the characteristics of SGR 1900+14. We have already pointed out that the properties of recurrent bursts remained practically unchanged (Mazets et al., 1999). No substantial variations in the neutron-star rotation period which could be associated with the outburst were observed (Kouveliotou et al., 1999). At the same time the profile of the 5.16-s pulsations in the weak persistent X-ray flux did undergo changes. Indeed, the multi-peak pulsations seen in May 1998 were replaced, judging from the 1998 August 28 observations, by a single-peak pattern (Kouveliotou et al., 1999). This transition may have been very fast, during the pulsation stage of the outburst (see Fig. 7).

Detection of two giant outbursts in different sources during $t = 20$ years undoubtedly implies that such bursts must be recurrent events. As pointed out more than once (Kouveliotou et al., 1994; Norris et al., 1991), the number N of neutron stars in the Galaxy residing at any one time in the SGR stage, should be small, ~ 7 . Accordingly, the average time interval τ between giant outbursts in the same repeater should not be large. Assuming k bursts to occur in N sources in t years, rough estimates made by the maximum likelihood method yield $\tau \sim Nt/k \sim 50 - 100$ years.

It should be pointed out that the sensitivity of present-day γ -ray burst detectors is high enough to permit observation of the initial pulses in giant outbursts from soft gamma repeaters in the Local-Group of galaxies, primarily in the Andromeda Galaxy. For the distance to such sources of ~ 700 kpc, the bursts should appear as short, ~ 0.2 -s long, spikes with an intensity $\sim 10^{-6}$ erg cm $^{-2}$. Their occurrence frequency should be of the order of one event per decade. Given a certain luck, such bursts could be detected and localized.

A neutron star in the stage of active soft gamma repeater expends its energy in supporting emission of a soft X-ray source, giant outbursts, and weaker recurrent bursts. To maintain such an activity during $\sim 10^4$ years, the initial energy store in the source should be at least 10^{47} erg.

The authors thank G. M. Gorodinskii, A. A. Kolchin, and V. V. Lebedev for their assistance with the laboratory calibration of the equipment.

Support of the Russian Space Agency and Russian Basic Research Foundation (Grant 99-02-17031) is gratefully acknowledged.

REFERENCES

Aptekar, R.L., et al. 1995, *Space Science Rev.*, 71, 265

Band, D., et al. 1993, *ApJ*, 413, 281

Case, G.L., Bhattacharya, D. 1998, *ApJ*, 504, 761

Cline, T.L., Mazets, E.P., & Golenetskii, S.V. 1998, *IAU Circ.* 7002

Fenimore, F.E., Klebesadel, R.W., & Laros, J.G. 1996, *ApJ*, 460, 964

Feroci, M., et al. 1999, *ApJ*, 515, L9

Golenetskii, S.V., Ilyinskii, V.N., & Mazets, E.P. 1984, *Nature*, 307, 41

Hurley, K., et al. 1999, *Nature*, 397, 41

Kočki, S., Kočki, A., Ajdačić, V. 1973, *Nuclear Instruments and Methods*, 108, 297

Kouveliotou, C., et al. 1994, *Nature*, 368, 125

Kouveliotou, C., et al. 1999, *ApJ*, 510, L115

Mazets, E.P., et al. 1979a, *Nature*, 282, 587

Mazets, E.P., Golenetskii, S.V., & Guryan, Yu.A. 1979b, *Soviet. Astron. Lett.*, 5(No6), 343

Mazets, E.P., et al. 1982, *Ap&SS*, 84, 173

Mazets, E.P., et al. 1999, *Astronomy Letters*, in press

Norris, J.P., Hertz, P., & Wood, K.S. 1991, *ApJ*, 366, 240

Rothschild, R., Kulkarni, S., & Lingenfelter R. 1994, *Nature*, 368, 432

Thompson, C. & Dunkan, R.C. 1995, *MNRAS*, 275, 255

Table 1. Comparative characteristics of the giant outbursts

	SGR 1900+14 $E_\gamma > 15$ keV	SGR 0526-66 $E_\gamma > 30$ keV
Giant outburst	August 27, 1998	March 5, 1979
Precursor	$T - T_0 = -0.45$ s $kT \sim 20$ keV	?
Initial pulse		
Duration	~ 0.35 s	~ 0.25 s
Steep rise time	< 4 ms	< 2 ms
Exponential falloff	$\tau_1 \sim 35$ ms	$\tau_1 \sim 40$ ms
Peak flux F , $erg\ cm^{-2}\ s^{-1}$	$> 3.1 \times 10^{-2}$	1×10^{-3}
Fluence S , $erg\ cm^{-2}$	$> 5.5 \times 10^{-3}$	4.5×10^{-4}
Spectral parameter kT , evolution	300 – 20 keV	~ 500 keV
Single wave		
Time interval, $T - T_0$	$\sim 0.35 - 0.8$ s	$\sim 0.25 - 1.5$ s
Oscillations, quasiperiod P	~ 0.08 s	~ 0.15 s
Peak flux F , $erg\ cm^{-2}\ s^{-1}$	$\sim 1.5 \times 10^{-3}$	$\sim 3 \times 10^{-5}$
Fluence S , $erg\ cm^{-2}$	$\sim 3 \times 10^{-4}$	$\sim 4 \times 10^{-5}$
Spectral parameter kT , evolution	20 – 250 keV	~ 30 keV
Tail		
Exponential decay	$\tau_2 \sim 90$ s	$\tau_2 \sim 100$ s
Period P	5.16 s	8.0 s
Fluence S , $erg\ cm^{-2}$	4.2×10^{-3}	1×10^{-3}
Spectral parameter kT	~ 20 keV	~ 30 keV
Recurrent bursts		
Observations	May 1998 - January 1999	March 1979 - April 1983
Duration	$\sim 0.1 \div 4$ s	$\sim 0.1 \div 9$ s
Peak flux F , $erg\ cm^{-2}\ s^{-1}$	$2 \times 10^{-6} \div 3 \times 10^{-5}$	$1 \times 10^{-6} \div 7 \times 10^{-6}$
Fluence S , $erg\ cm^{-2}$	$2 \times 10^{-7} \div 5 \times 10^{-5}$	$1.5 \times 10^{-7} \div 2 \times 10^{-5}$
Spectral parameter kT	$20 \div 30$ keV	$30 \div 35$ keV

Table 2. Luminosity and energy release in SGR 1900+14 and SGR 0526-66

	SGR 1900+14 $E_\gamma > 15$ keV	SGR 0526-66 $E_\gamma > 30$ keV
Distance	10 kpc ^(a)	55 kpc
Giant outburst	August 27, 1998	March 5, 1979
Initial pulse		
Energy release Q , <i>erg</i>	$> 6.8 \times 10^{43}$	1.6×10^{44}
Peak luminosity L , <i>erg s⁻¹</i>	$> 3.7 \times 10^{44}$	3.6×10^{44}
Tail		
Energy release Q , <i>erg</i>	5.2×10^{43}	3.6×10^{44}
Total energy release Q, <i>erg</i>	$> 1.2 \times 10^{44}$	5.2×10^{44}
Recurrent bursts		
Observations	May 1998 - January 1999	March 1979 - April 1983
Energy release Q , <i>erg</i>	$2 \times 10^{39} \div 6 \times 10^{41}$	$5 \times 10^{40} \div 7 \times 10^{42}$
Peak luminosity L , <i>erg s⁻¹</i>	$2 \times 10^{40} \div 4 \times 10^{41}$	$3 \times 10^{41} \div 3 \times 10^{42}$
X-Ray source		
Luminosity L , <i>erg s⁻¹</i>	$\sim 10^{36}$ ^(b)	$\sim 10^{35}$ ^(c)

(a) Case, Bhattacharya, 1998

(b) Kouveliotou et al., 1999

(c) Rothschild, Kulkarni, Lingenfelter, 1994

FIGURE CAPTIONS

Fig. 1.— The giant 1998 August 27 outburst. Intensity of the $E_\gamma > 15$ keV radiation.

Fig. 2.— The initial phase of the burst recorded in three energy windows. Total detector overload for $T - T_0 < 0.2$ s.

Fig. 3.— Count rates in three energy windows G1, G2, and G3 as functions of load (irradiation with a broad line with an energy of ~ 100 keV). Symbols – laboratory measurements. Solid lines – numerical simulation. Dashed line – a plot of the standard relation $n(N, \tau)$ for $\tau = 2.85 \times 10^{-6}$ s.

Fig. 4.— Imitation of a short burst caused by a nuclear interaction in the NaI(Tl) scintillator with the release of enormous energy $\sim 2.5 \times 10^3$ GeV. The characteristic features of the overload are similar to those in the initial phase of the August 27 event.

Fig. 5.— Energy loss spectra for the interval $T - T_0 = 0.256 - 1.280$ s display extremely strong distortions of the incident photon spectrum because of pulse superposition. The incident spectrum within the interval $T - T_0 = 0.512 - 0.768$ s is obviously substantially harder.

Fig. 6.— Reconstructed time history for the first second of the burst: radiation intensity with $E_\gamma > 15$ keV and calculated parameter kT . The horizontal dashed line specifies the low intensity threshold causing total overload. The sloped line is a plot of the relation $\exp(-t/\tau)$ for $\tau_1 = 35$ ms.

Fig. 7a.— Time profile of the pulsating stage. The vertical dashed lines are spaced by the pulsation period of 5.16 s.

Fig. 7b.— Time profile of the pulsating stage (continuation).

Fig. 7c.— Time profile of the pulsating stage (continuation).

Fig. 8.— Energy spectra of the burst pulsating stage.

Fig. 9.— Time and energy characteristics of the March 5 event.

Fig. 10.— Time and energy characteristics of the August 27 event.

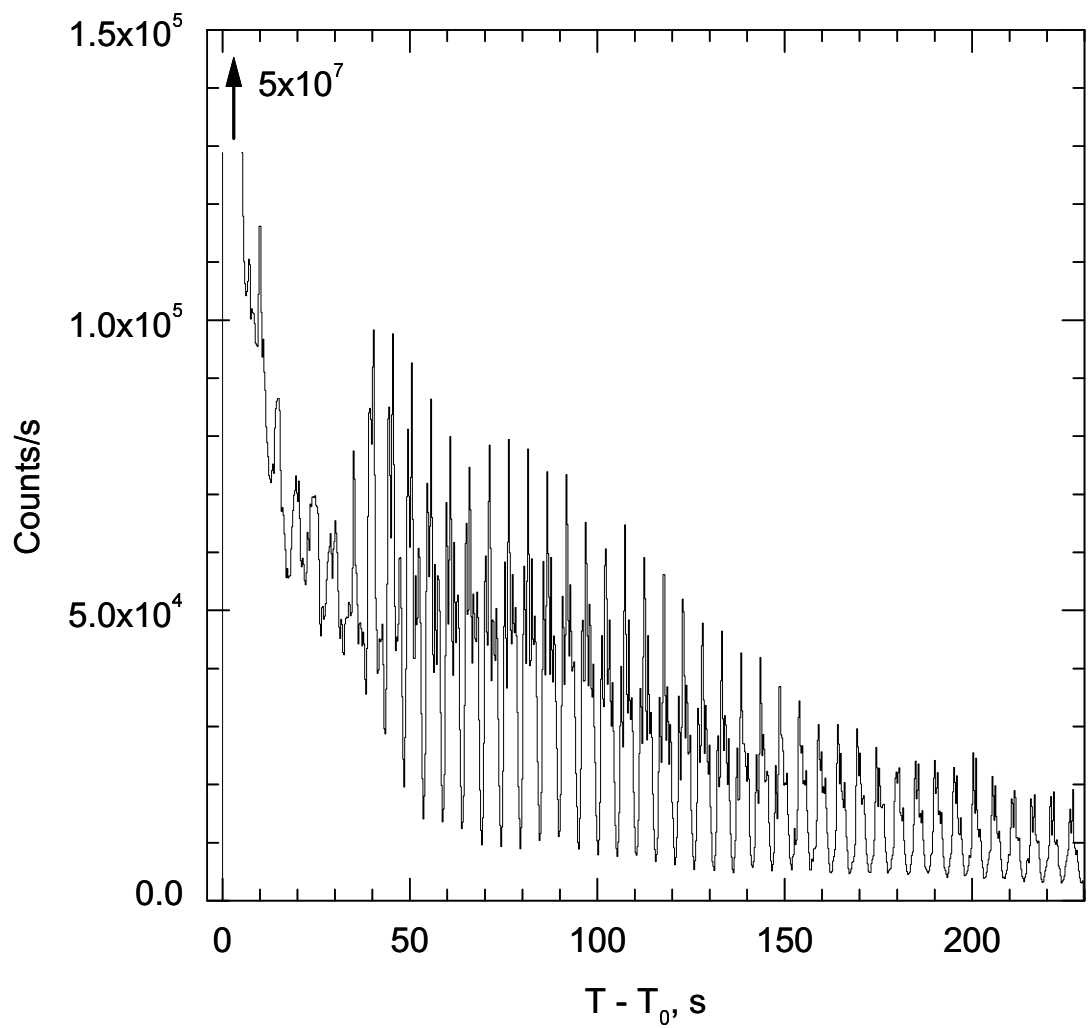


Fig. 1. The giant 1998 August 27 outburst. Intensity of the $E_{\gamma} > 15$ keV radiation.

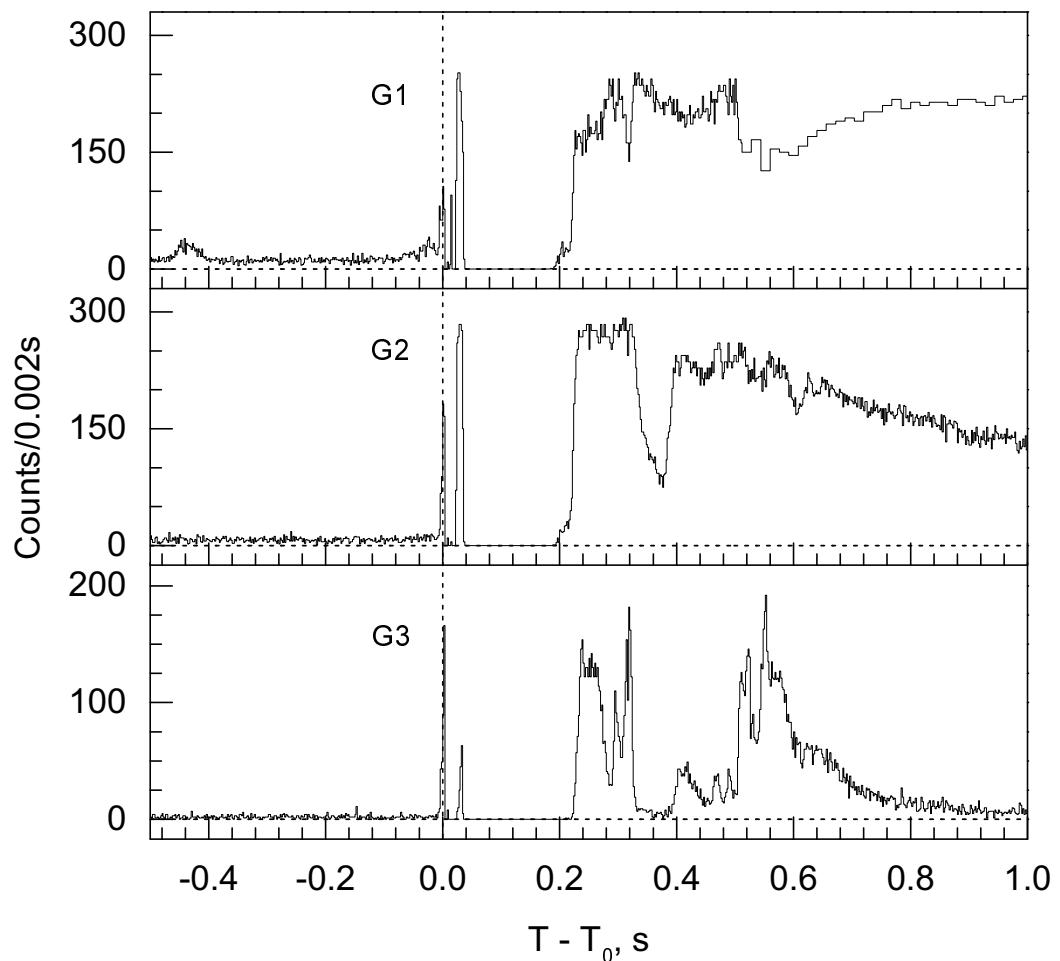


Fig. 2. The initial phase of the burst recorded in three energy windows. Total detector overload for $T - T_0 < 0.2$ s.

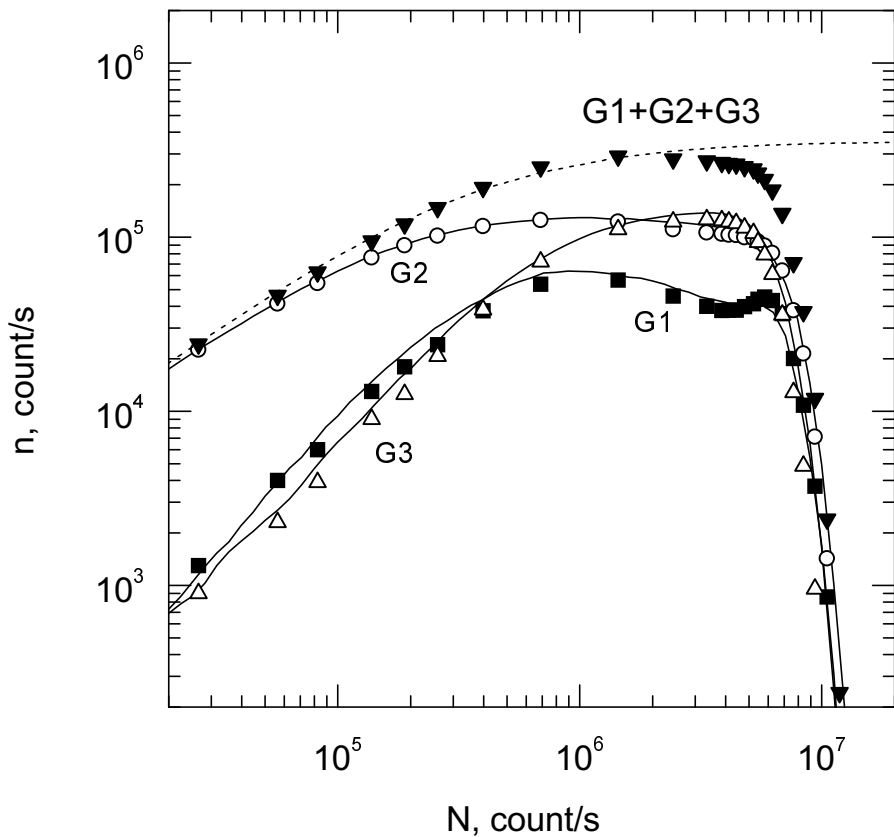


Fig. 3. Count rates in three energy windows G1, G2 and G3 as functions of load (irradiation with a broad line with an energy of ~ 100 keV).
 Symbols - laboratory measurements.
 Solid lines - numerical simulation.
 Dashed line - a plot of the standard relation $n(N, \tau)$ for $\tau = 2.85 \cdot 10^{-6} \text{ s}$.

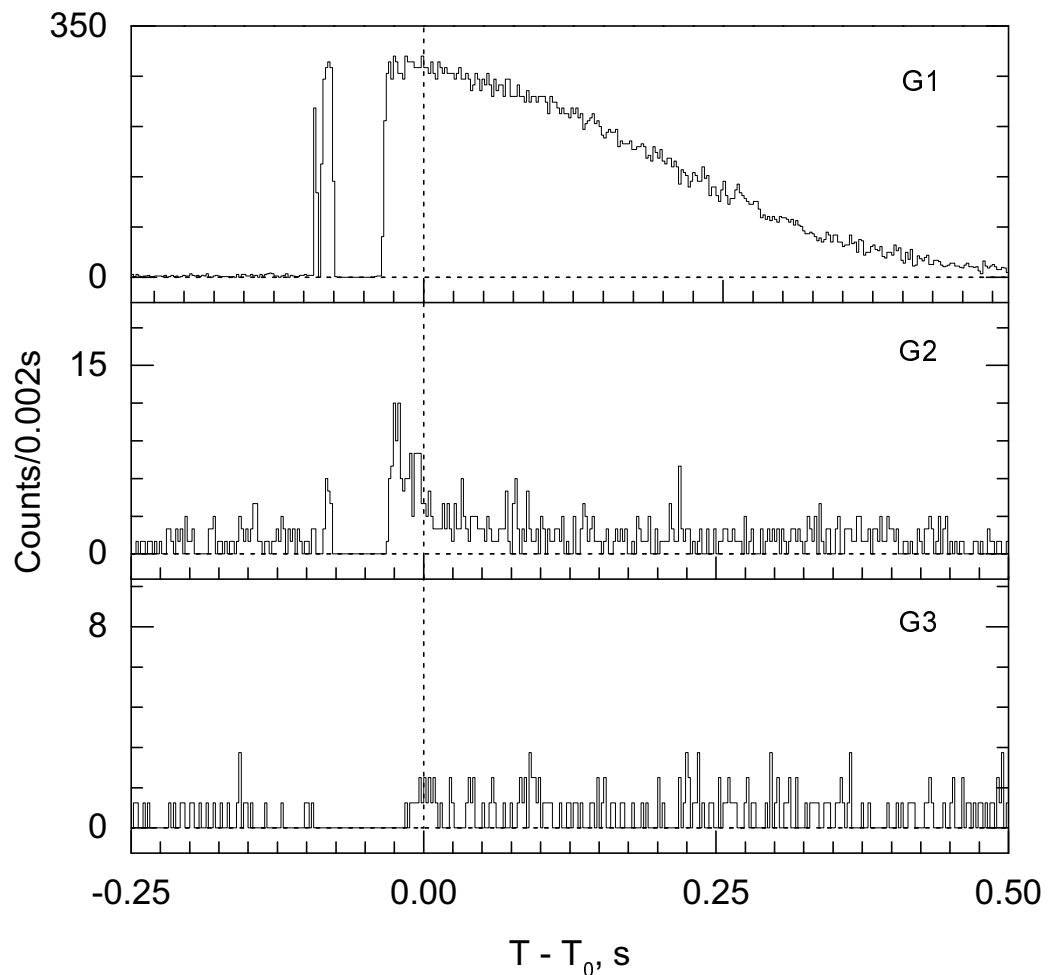


Fig. 4. Imitation of a short burst caused by a nuclear interaction in the NaI(Tl) scintillator with the release of enormous energy $\sim 2.5 \cdot 10^3 \text{ GeV}$. The characteristic features of the overload are similar to those in the initial phase of the August 27 event.

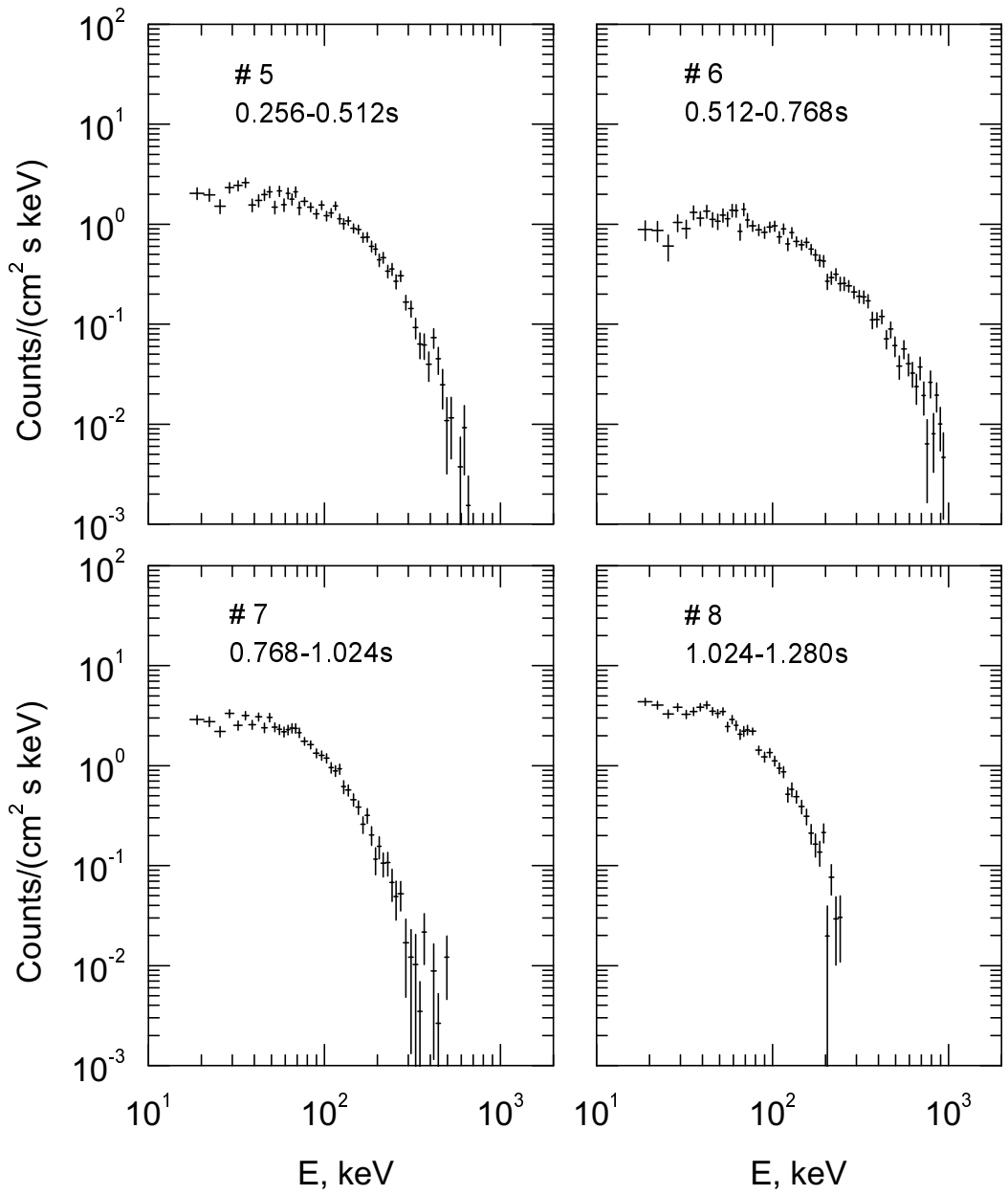


Fig. 5. Energy loss spectra for the interval $T - T_0 = 0.256 - 1.280$ s display extremely strong distortions of the incident photon spectrum because of pulse superposition. The incident spectrum within the interval $T - T_0 = 0.512 - 0.768$ s is obviously substantially harder.

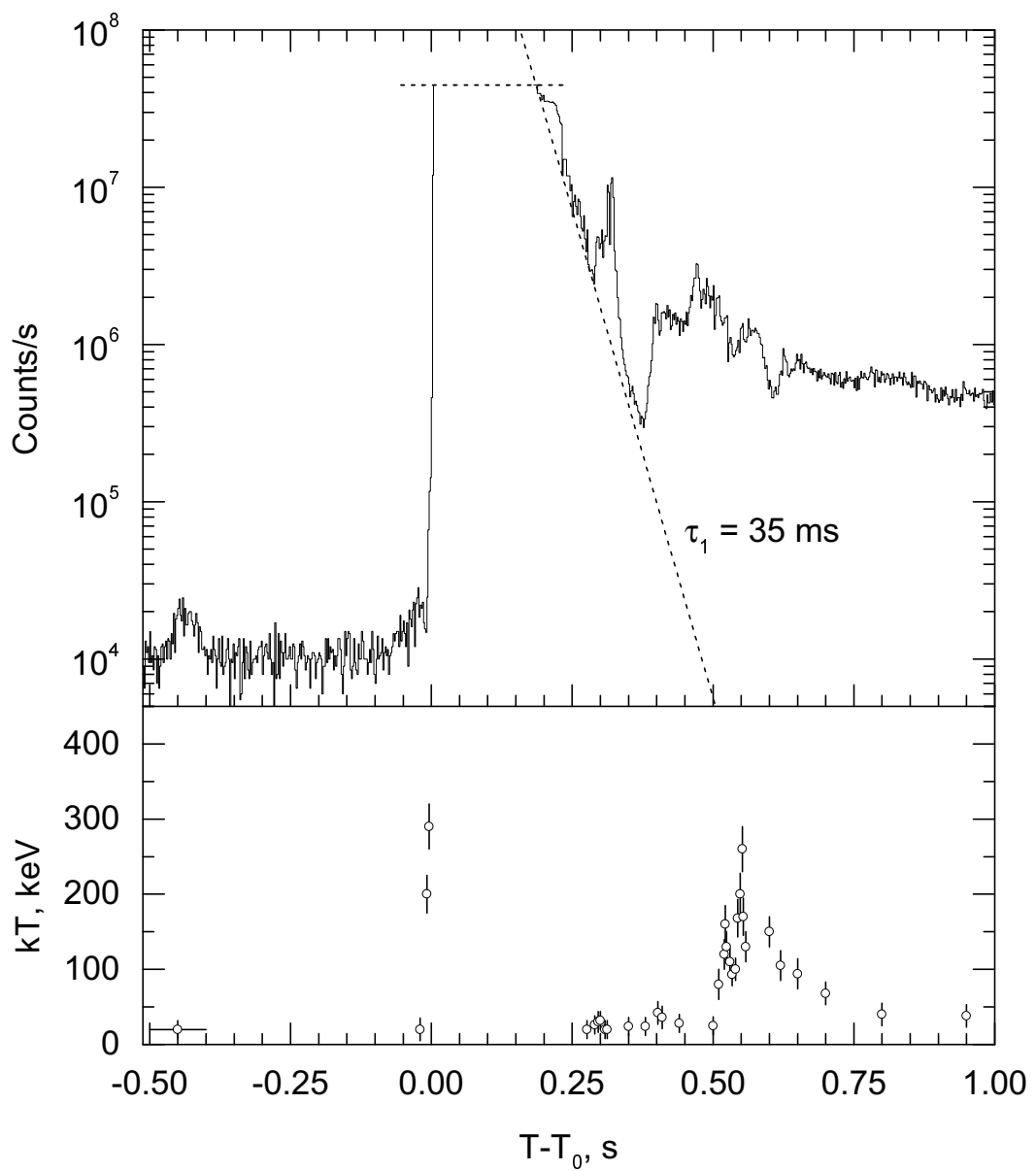


Fig. 6. Reconstructed time history for the first second of the burst: radiation intensity with $E_\gamma > 15$ keV and calculated parameter kT . The horizontal dashed line specifies the low intensity threshold causing total overload. The sloped line is a plot of the relation $\exp(-t/\tau)$ for $\tau_1 = 35$ ms.

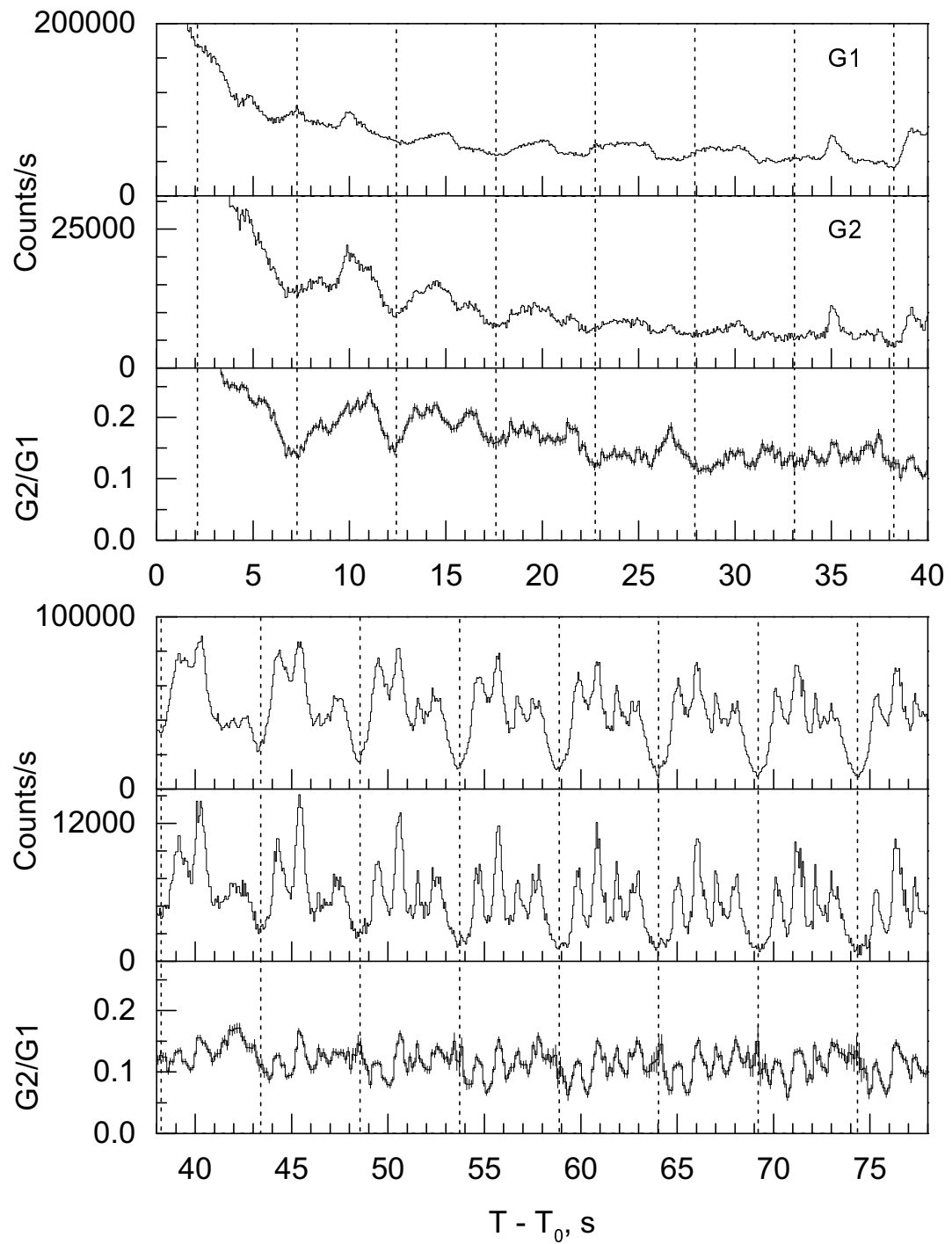


Fig. 7a. Time profile of the pulsating stage. The vertical dashed lines are spaced by the pulsation period of 5.16 s.

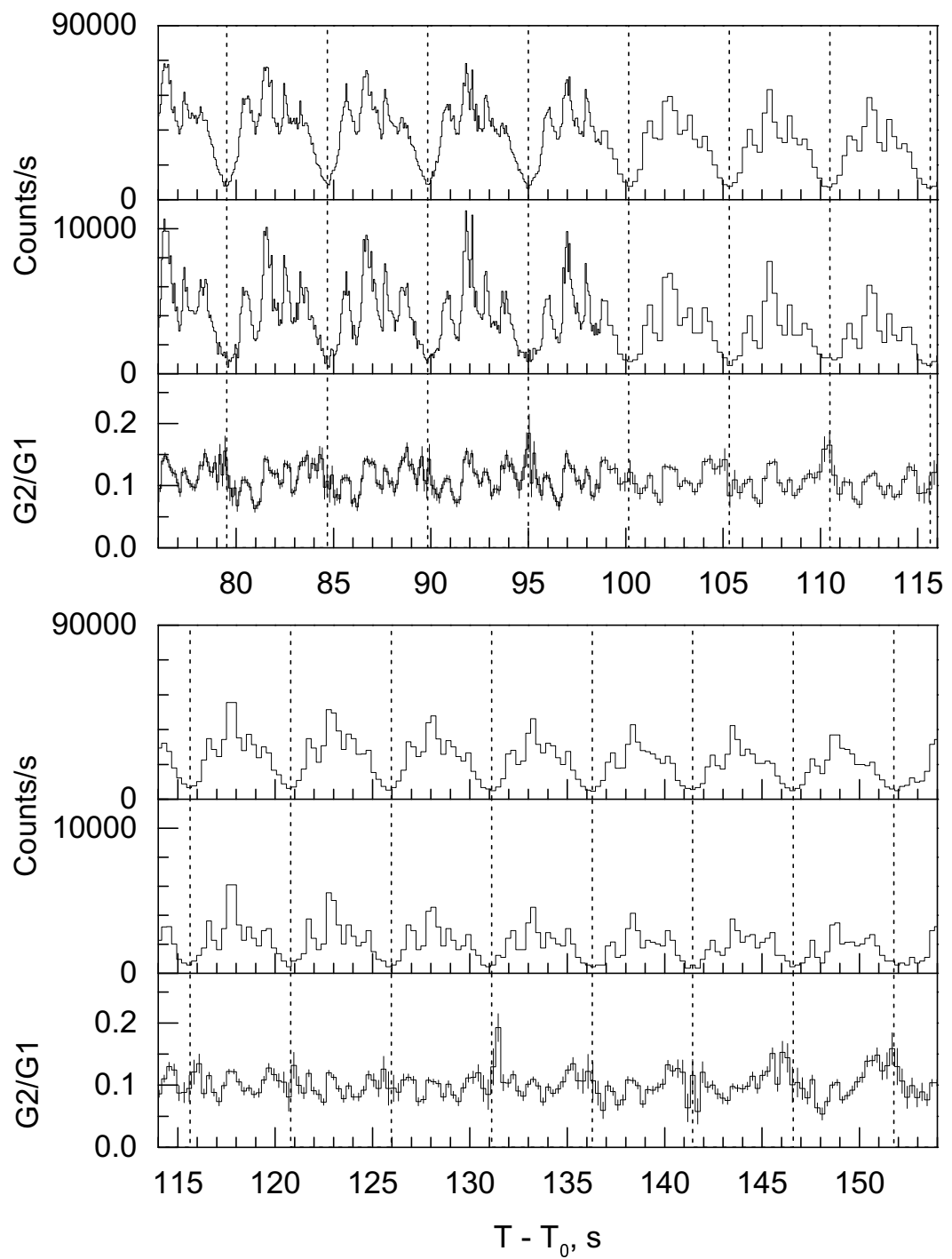


Fig. 7b. Time profile of the pulsating stage (continuation).

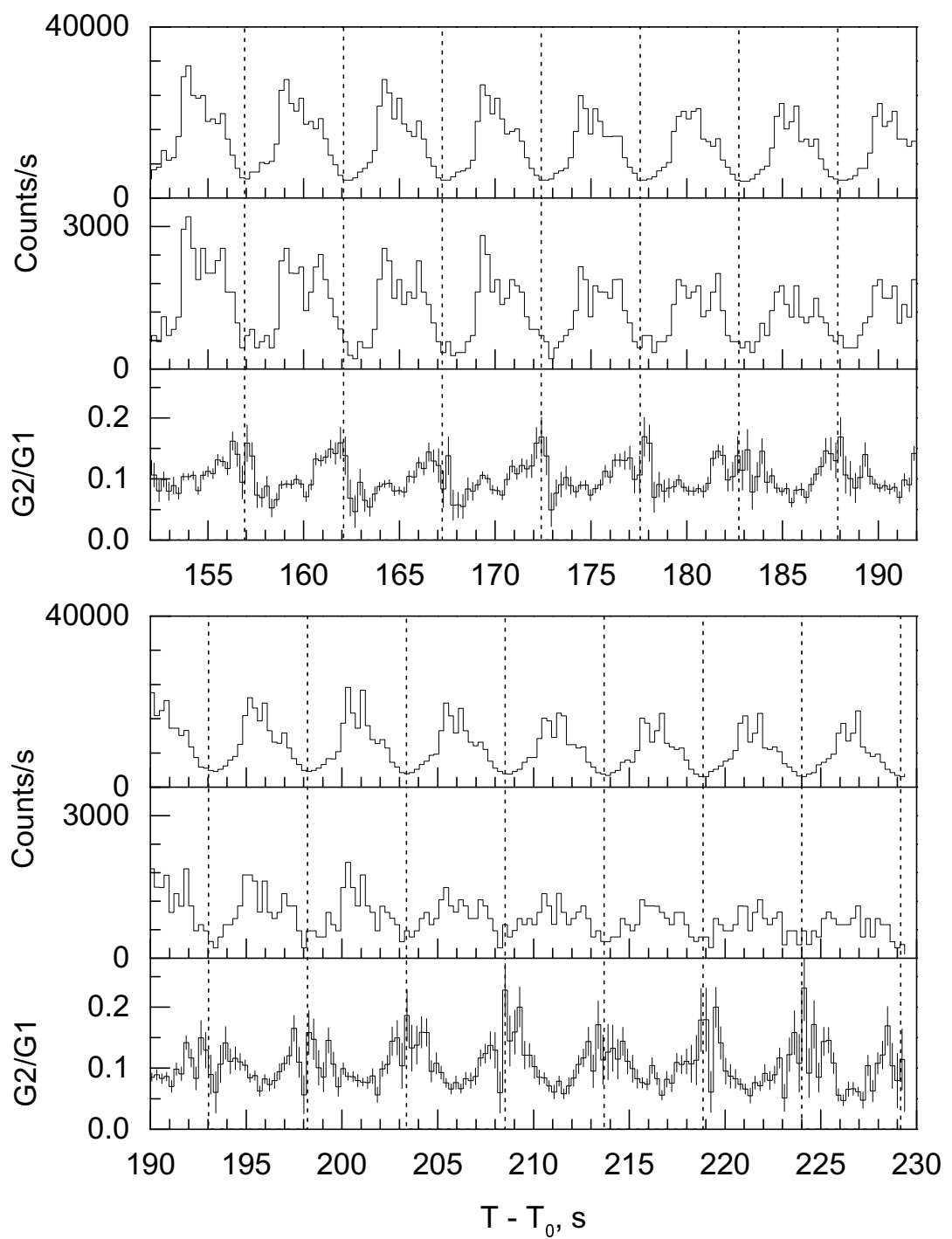


Fig. 7c. Time profile of the pulsating stage (continuation).

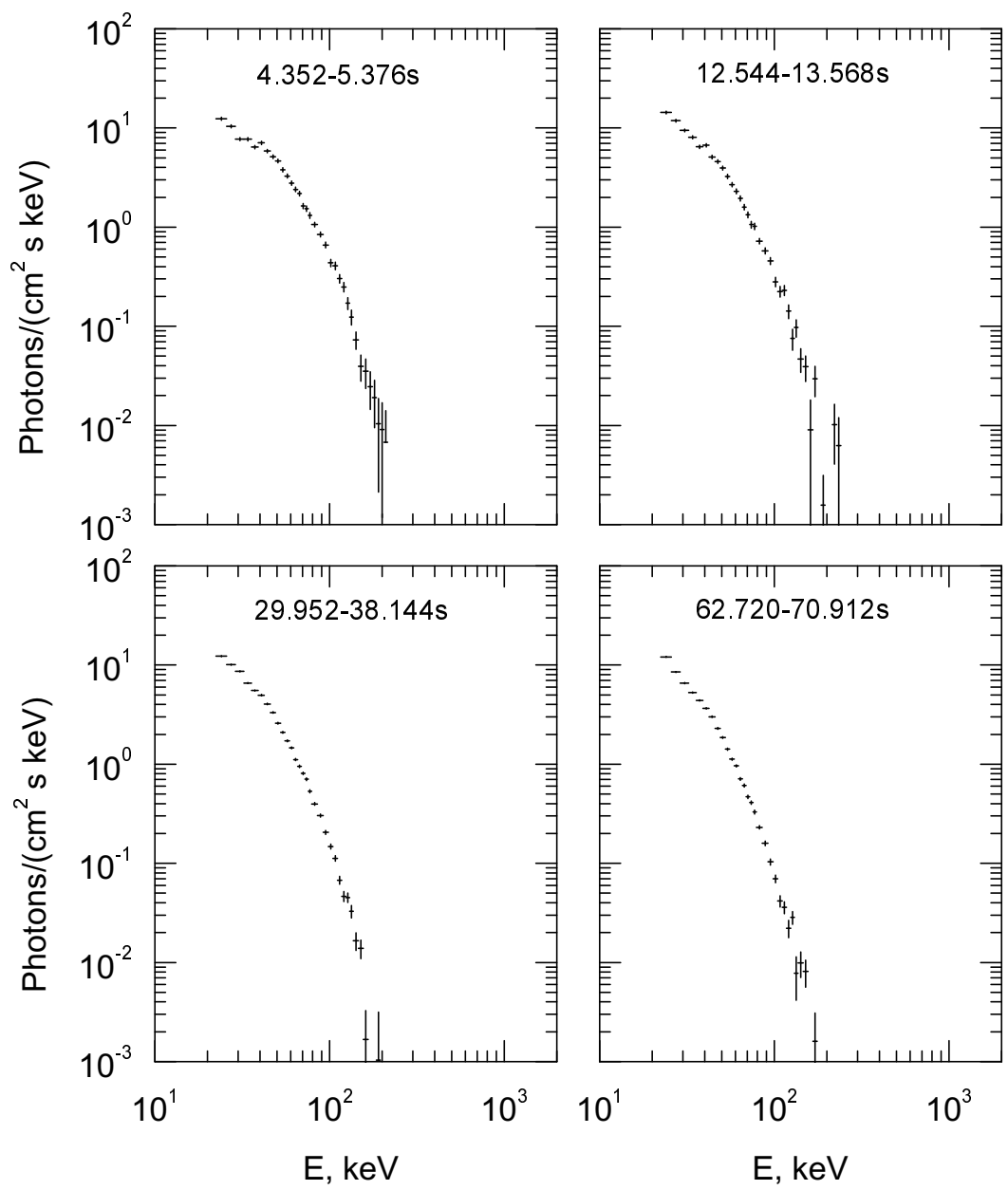


Fig. 8. Energy spectra of the burst pulsating stage.

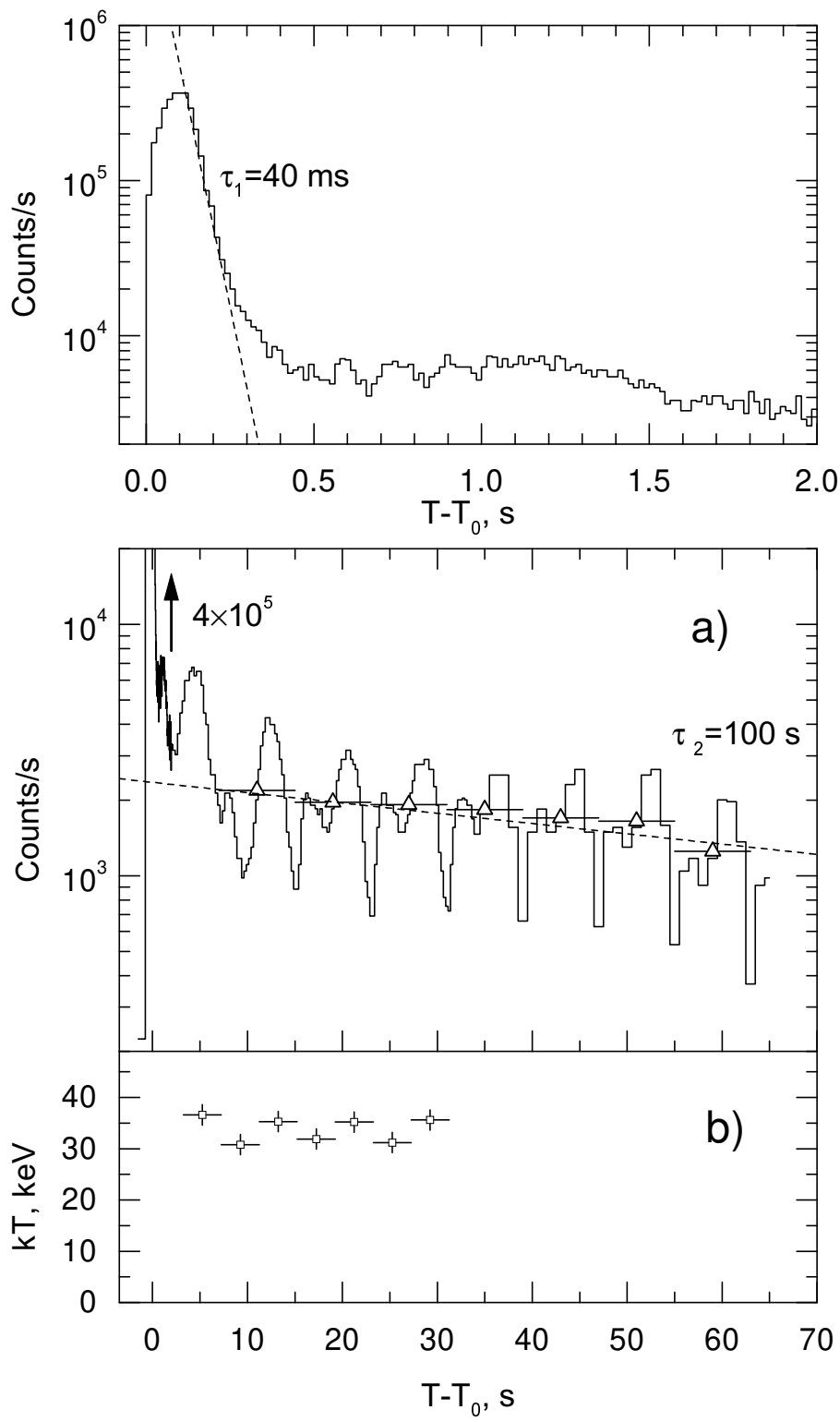


Fig. 9. Time and energy characteristics of the 5 March event.

Top: The initial phase of the outburst. The sloped line is a plot of the relation $\exp(-t/\tau)$ for $\tau_1 = 40$ ms.

Bottom: **a)** Background subtracted light curve of the outburst. Horizontal sections with triangles specify count rates averaged over the period. The sloped dashed line is a plot of $\exp(-t/\tau)$ relation for $\tau_2 = 100$ s.

b) Horizontal sections with squares specify kT averaged over the period.

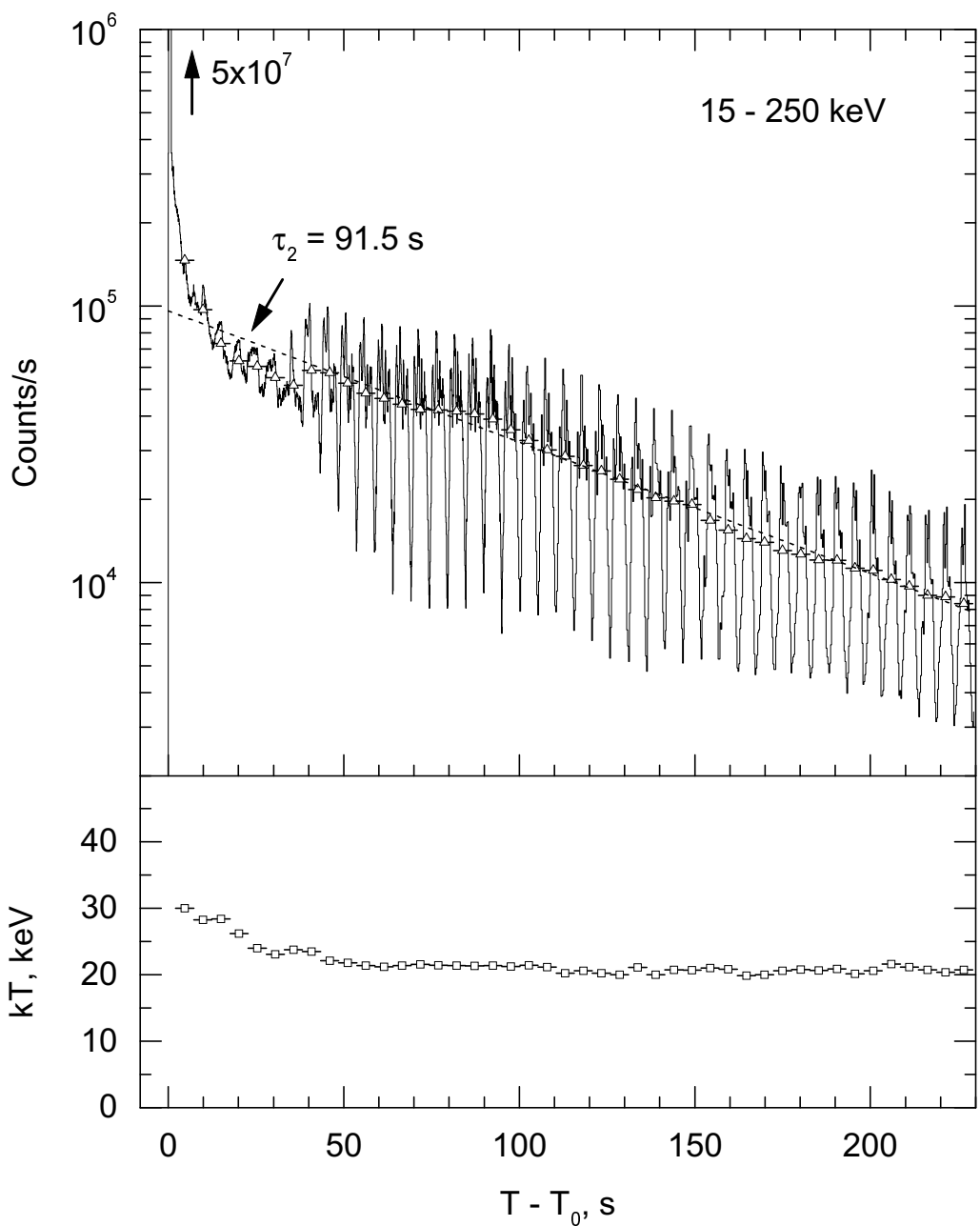


Fig. 10. Time and energy characteristics of the August 27 event.

Top: Background subtracted light curve of the outburst. Horizontal sections with triangles specify count rates averaged over the period. The sloped dashed line is a plot of $\exp(-t/\tau)$ for $\tau_2 = 91.5$ s.

Bottom: Horizontal sections with squares specify kT averaged over the period.

